frontiers | Frontiers in Marine Science

TYPE Original Research
PUBLISHED 16 August 2022
DOI 10.3389/fmars.2022.932184

OPEN ACCESS

EDITED BY
Michelle Jillian Devlin,
Centre for Environment, Fisheries and Aquaculture Science (CEFAS), United Kingdom

REVIEWED BY
Heng Lyu,
Nanjing Normal University, China
Zhigang Cao,
Nanjing Institute of Geography and Limnology, Chinese Academy of Sciences (CAS), China

*CORRESPONDENCE
Emmanuel Devred
Emmanuel.devred@dfo-mpo.gc.ca

SPECIALTY SECTION
This article was submitted to Marine Ecosystem Ecology, a section of the journal Frontiers in Marine Science

RECEIVED 29 April 2022
ACCEPTED 12 July 2022
PUBLISHED 16 August 2022

CITATION
Devred E, Perry T and Massicotte P (2022) Seasonal and decadal variations in absorption properties of phytoplankton and non-algal particulate matter in three oceanic regimes of the Northwest Atlantic. *Front. Mar. Sci.* 9:932184. doi: 10.3389/fmars.2022.932184

Seasonal and decadal variations in absorption properties of phytoplankton and non-algal particulate matter in three oceanic regimes of the Northwest Atlantic

Emmanuel Devred[1]*, Tim Perry[1] and Philippe Massicotte[2]

[1]Ocean and Ecosystem Sciences Division, Bedford Institute of Oceanography, Fisheries and Oceans Canada, Dartmouth, NS, Canada, [2]Takuvik Joint International Laboratory, Laval University (Canada)-CNRS (France), Département de biologie et Québec-Océan, Université Laval, Québec, QC, Canada, Québec, QC, Canada

Seasonal and inter-annual absorption properties of phytoplankton and non-algal particulate matter were studied in relation to phytoplankton biomass, as indexed by chlorophyll-a concentration, and presence of diatoms, as indexed by fucoxanthin concentration, using a 20-year time series of *in situ* data collected in the Northwest Atlantic. We found significant differences in the spatiotemporal variations of the bio-optical properties for three oceanic regimes: mesotrophic (Scotian Shelf), oligotrophic (Northwest Atlantic Basin, NAB), and subartic (Labrador Sea). The Scotian Shelf and NAB exhibited similar phenology with the spring and autumn blooms associated with low phytoplankton specific absorption, while only relatively high fucoxanthin concentration occurred in spring. The NAB showed a smaller seasonal variation than the Scotian Shelf in agreement with its oceanic conditions. The Labrador Sea showed a single phytoplankton bloom in spring followed by a continuous decrease in biomass the rest of the year. The relationship between phytoplankton absorption coefficient at 443 nm and chlorophyll-a concentration was consistent with other studies with coefficients that were region-dependent. Absorption by non-algal particulate matter remained between 5% and 60% of phytoplankton absorption with a mean of 15%. The slope of the non-algal particulate absorption varied with seasons and regions and appeared to depend on the trophic status with high values (i.e., up to 0.04) occurring during bloom conditions. We also introduced a new index, the phytoplankton apparent absorption wavelength (*PAAW*), a wavelength-weighted sum of absorption expressed in nanometers that provides information on the phytoplankton biomass and assemblage in a simple manner. Time series analysis of the *PAAW* revealed a decrease of this property in spring on the Scotian Shelf, NAB, and Labrador Sea and an

increase in autumn on the Scotian Shelf and NAB, suggesting a shift in these ecosystems.

KEYWORDS

phytoplankton, absorption, chlorophyll-a concentration, phytoplankton apparent absorption wavelength (PAAW), Northwest Atlantic, time series analysis

1 Introduction

Inherent optical properties (IOPs) of marine particulate and dissolved matter play an important role in the optical budget of marine waters, which, in turn, provides important information on light regime in the water column, trophic status, and functioning of the marine ecosystem. In particular, the absorption coefficients of phytoplankton (a_ϕ) and non-algal particles (*NAP*, a_{NAP}) have been extensively studied in the open ocean (e.g., Gordon and McCluney, 1975; Morel and Bricaud, 1981; Mobley, 1994; Bricaud et al., 1995; Cleveland, 1995; Bricaud et al., 1998; Ciotti et al., 2002; Bricaud et al., 2004; Devred et al., 2006; Bricaud et al., 2010; Brewin et al., 2011), and coastal (Babin et al., 2003) and polar aquatic environments (Matsuoka et al., 2014; Ferreira et al., 2017) to understand their variation in space and time in conjunction with phytoplankton dynamics. The knowledge of phytoplankton and *NAP* absorption properties is key to the understanding and quantification of a wide range of bio-optical and ecological issues such as primary production (Marra et al., 2007) and determination of phytoplankton functional types (Nair et al., 2008).

In the context of satellite ocean color, the retrieval of chlorophyll-a concentration, [Chl-a], is often addressed using empirical relationships between remote sensing reflectance and [Chl-a] (O'Reilly et al., 1998), which treat the ocean optical properties *de facto* as a black box (IOCCG, 2006). The use of IOPs in semi-analytical models and knowledge of the inverse problem provide a more robust, qualitative, and quantitative relationship between reflectance and IOPs, which translates into more accurate retrievals of biogeochemical parameters, emphasizing the need to characterize the spectral dependence of phytoplankton and NAP absorption (IOCCG, 2006). The use of phytoplankton absorption is not restricted to satellite applications, and its field of applications is far-reaching as knowledge on its magnitude and spectral variation in natural water samples informs on biomass (e.g., Gordon and McCluney, 1975; Morel and Bricaud, 1981; Prieur and Sathyendranath, 1981; Bricaud et al., 1995; Cleveland, 1995; Bricaud et al., 1998; Babin et al., 2003; Matsuoka et al., 2014; Ferreira et al., 2017), pigment composition and concentration (Hoepffner and Sathyendranath, 1991; Sathyendranath et al., 2001; Chazottes et al., 2006; Bricaud et al., 2007; Chase et al., 2013), and the packaging effect (Duysens, 1956; Kirk, 1976; Mitchell and Kiefer, 1988; Bricaud et al., 1995; Bricaud et al., 2004), which helps determine phytoplankton assemblage and size distribution (Fujiki and Tagushi, 2002; Ciotti et al., 2002; Sathyendranath et al., 2004; Devred et al., 2006; Devred et al., 2011; Brewin et al., 2011). Because phytoplankton absorption is characterized by a wide peak around 443 nm and a sharp maximum around 675 nm, empirical relationships usually focus on these two wavelengths rather than fully exploiting the spectral information contained in absorption measurements (Bricaud et al., 1995; Babin et al., 2003; Aiken et al., 2007). Phytoplankton absorption is also used in direct (Marra et al., 2007) and indirect (Morel, 1978; Kyewalyanga et al., 1997) computation of primary production.

The relationship between phytoplankton biomass and absorption has been widely studied and a consensus has been reached on its formulation (i.e., power law), whose coefficients might change in time and space (Bricaud et al., 1995; Bricaud et al., 1998; Bricaud et al., 2004). Studies on the relationship between phytoplankton and non-algal particle absorption remain scarce in open oceans, despite the role of *NAP* in the absorption budget and its production by plankton grazing (Shuman and Lorenzen, 1975; Head and Horne, 1993), which inform on the trophic status. While the ratio of a_ϕ and a_{NAP} may be location dependent (Sosik and Mitchell, 1992), it has been found to be as low as 10% at the surface in open oceans and reach 20% to 30% at depth (Bricaud et al., 1998), while it can dominate the absorption budget in coastal areas (Babin et al., 2003; Williams et al., 2018; Kratzer and Moore, 2018) and river delta (Retamal et al., 2008). Detailed knowledge on the seasonal and long-term variation of phytoplankton and non-algal particle absorption remains a gap in the understanding of the functioning of the marine ecosystem and the factors that affect it, in particular in case 1 waters (Morel and Prieur, 1977) where it dominates the absorption budget (Oubelkheir et al., 2007; Mascarenhas et al., 2017).

In the current study, we aim at addressing this gap for the Northwest Atlantic (NWA) using a 20-year time series of a_ϕ and a_{NAP} collected during the Department of Fisheries and Oceans Canada monitoring programs, which happened all year long in three oceanic regimes: (1) a mid-latitude shelf environment, with

high seasonal variations in phytoplankton biomass and associated properties: the Scotian Shelf; (2) an oligotrophic environment, with low biomass and a more subtle seasonal cycle: the NAB; and, finally, (3) a subarctic environment with a delayed phytoplankton spring growth: the Labrador Sea. Several studies evidenced the optical signature of phytoplankton in the Northwest Atlantic (Stuart et al., 1998; Sathyendranath et al., 2001; Sathyendranath et al., 2004; Devred et al., 2006; Devred et al., 2011) and in particular in the Labrador Sea (Stuart et al., 2000; Cota et al., 2003), but using limited datasets. These studies showed that, on average, diatom-dominated water samples had a different absorption spectrum than assemblages made of a phytoplankton mixed population due to different pigment composition and packaging effect, resulting in a lower absorption per unit of chlorophyll-a (Sathyendranath et al., 2004). Building on these previous studies, our objectives are to (1) describe and interpret the seasonal variation in both magnitude and spectral signature of phytoplankton and *NAP* absorption coefficients in relation to phytoplankton biomass and presence of diatoms as indicated by the fucoxanthin pigment (Jeffrey and Vesk, 1997), (2) study the relationship between phytoplankton and *NAP* absorption, and (3) analyze time series of phytoplankton and *NAP* absorption to detect significant changes that may have occurred over the 20 years of observations. Our secondary objectives are (1) to introduce a new index, the phytoplankton apparent absorption wavelength (*PAAW*), which summarizes all the spectral information contained in a given phytoplankton absorption spectrum into a single number (nm); (2) to detect possible changes in *PAAW* at the seasonal and interannual scale; and (3) to assess if the extensive sampling conducted over the last 20 years has captured the variability in phytoplankton and *NAP* absorption.

2 Materials and methods

2.1. Study area and sampling

Since 1999, the Department of Fisheries and Oceans Canada (DFO) has been conducting annual surveys in the Northwest Atlantic as part of the Atlantic Zone and Atlantic Offshore Zone monitoring programs (Therriault et al., 1998; Pepin et al., 2005). Each year, in spring, sometimes between April and June depending on ship availability and weather, about 100 stations are sampled on the Scotian Shelf and Gulf of Maine regions and 28 stations are sampled in the Labrador Sea along a transect that spans from the Labrador Shelf (Canada) to the Greenland Shelf (Denmark), crossing the Labrador Basin (Figure 1). The spring cruise on the Scotian Shelf is repeated in the autumn from mid-October to mid-November. Fish surveys that happened during winter and summer opportunistically provided additional water samples. For this study, a total of 3,279 sampling events were compiled and grouped into three bioregions, namely, the Scotian Shelf, a temperate mesotrophic environment, the NAB, a temperate oligotrophic environment, and the Labrador Sea, a subarctic environment (see Supplementary Figure S1 for details on samples spatiotemporal distribution). The delineation of these bioregions was based on bathymetry (GEBCO2021) and the latitude as follows: (1) Scotian Shelf (bathymetry < 600 m and latitude < 48°N), (2) NAB (bathymetry < 600 m and latitude < 48°N), and (3) Labrador Sea (latitude < 48°N). Observations were further grouped into seasons based on the time of sampling (Supplementary Figure S1B): spring (March, April, and May, N = 1598), summer (June, July, and August, N = 369), autumn (September, October, and November, N = 1174), and winter (December, January, and February, N = 138). At each station, surface water (< 30 m) was collected to measure phytoplankton pigment composition and particulate absorption.

2.2. Data and laboratory analysis

2.2.1. Chlorophyll-a and fucoxanthin pigment concentration

Samples for pigment analysis were filtered at low pressure (< 10 dpi) on 25 mm WF/F Whatman filters (sterlitech Grade F Glass microfiber) with 0.2-µm mesh size and immediately flash frozen and stored in liquid nitrogen during the seagoing fieldwork. The volume of filtration varied between 0.25 and 1 L based on a visual inspection of the filter color to ensure that enough material was retained for analysis. Upon return to the Bedford Institute of Oceanography, the samples were stored inside a −80°C freezer until analysis in the laboratory. Pigment composition and concentration were measured on a Beckman–Coulter Gold High-Performance Liquid Chromatography (HPLC) system between 1998 and 2013, and on an Agilent 1200 HPLC system for samples collected between 2013 and 2020. Details on the HPLC method to extract and measure pigment concentration can be found in Head and Horne (1993) and Stuart and Head (2005). In this study, we limited the pigments to chlorophyll-a and derivative ([Chl-a] in mg m^{-3}) and fucoxanthin ([Fucox] in mg m^{-3}) concentration, the latter being used as a coarse indicator of diatom presence in samples (although the pigment is also present in some chrysophytes Jeffrey and Vesk, 1997).

2.2.2. Absorption coefficient of phytoplankton and non-algal particulate matter

Filtration for phytoplankton (a_ϕ) and non-algal particle (a_{NAP}) absorption coefficients was carried out simultaneously to the filtration for pigment analysis following the same protocol (i.e., filtration and storage method). Phytoplankton absorption coefficients between 350 and 750 nm were measured at 1-nm increments on a UV-Vis Shimadzu 2600i double beam with an integrating sphere in transmission mode. Only the visible part of

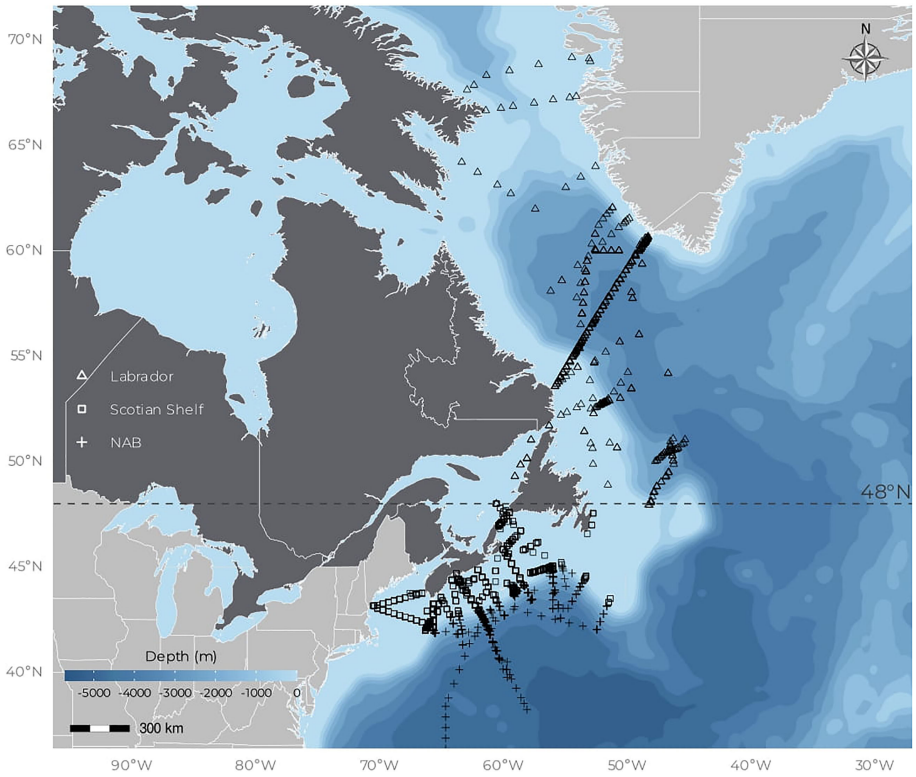

FIGURE 1
Location of samplings. The blue background indicates the bathymetry (see color bar in the bottom left panel). Dark gray corresponds to Canada and light gray corresponds to other countries (i.e., United States of America and Denmark).

the spectrum (400–700 nm) was used in the current study. Total particulate absorption coefficient (a_p) was measured first, after which the filter was soaked in hot methanol for 25 to 45 min to extract phytoplankton pigments. The absorption by non-algal particles, also referred to as detritus absorption, was then measured, and phytoplankton absorption was inferred by subtraction of a_{NAP} from a_p as described in Mitchell and Kiefer (1984) following modifications by Hoepffner and Sathyendranath (1991) and Kyewalyanga et al. (1997). The pathlength correction (i.e., the β-factor) was computed as in Stramski et al. (2015). Two quality control procedures were used to ensure the integrity of the absorption dataset; spectra were removed from further analysis if (1) negative values occurred between 350 and 400 nm and (2) the absorption coefficient at 410 nm was higher than that at 443 nm as in Devred et al. (2006). The slope of the exponential decrease of the particulate absorption spectrum, S_{NAP}, was computed as in Babin et al. (2003) by fitting Equation 1 to the data using the *nls()* function in R over the range 400 to 700 nm excluding the 400 to 480 nm and 620 to 700 nm ranges to avoid possible contamination by pigment remaining from the extraction:

$$a_{NAP}(\lambda) = a_{NAP}(443)(-S_{NAP}(\lambda - 443)) . \quad (1)$$

2.3. Statistical analysis

2.3.1. Phytoplankton apparent absorption wavelength

To summarize the spectral information contained in phytoplankton absorption measurements in a simple index, we used a method similar to that of Vandermeulen et al. (2020). The formulation of this index was initially proposed to maximize the utilization of the spectral information contained in remote sensing reflectance, and simply represents the weighted harmonic mean of a spectrum in opposition to the weighted arithmetic mean, which would emphasize the contribution from the red part of the spectrum (i.e., high wavelength). As pointed out by Vandermeulen et al. (2020), the index indicates the wavelength balance point around which the absorption spectrum is evenly distributed as absorption at all wavelengths contributed equally to the sum without spectral bias. Since we adopted this index to characterize the spectral shape of *in situ*

phytoplankton absorption, we named it *PAAW*, which was calculated as follows:

$$PAAW = \frac{\sum_{\lambda=400}^{\lambda=700} a_\phi(\lambda)}{\sum_{\lambda=400}^{\lambda=700} a_\phi(\lambda)/\lambda}$$

where $a_\phi(\lambda)$ is the phytoplankton absorption coefficient at the wavelength λ (nm).

2.3.2. Linear regression and trend analysis

The relationship between phytoplankton absorption coefficient at a given wavelength and [Chl-a] was derived using a type 2 linear regression on the log10-transformed data (when required to achieve normality). Time series analyses of a_ϕ (443), *PAAW*, a_{NAP}(443), and the a_ϕ(443): a_{NAP}(443) ratio were performed on data collected in spring and autumn (except for the Labrador Sea in autumn only), as there were not sufficient years with data in winter and summer to obtain statistically reliable trends. Trends for each property were computed for the entire NW Atlantic, the three individual regions (i.e., Scotian Shelf, NAB, and Labrador Sea), the three individual regions in spring only, and, finally, the Scotian Shelf and NAB in autumn adding up to a total of eight subdivisions of the original dataset from the most global to regional/seasonal ones. The annual mean properties were computed for a given dataset, and their long-term (i.e., 20 years) trends were derived using a weighted linear model [*lm*() in R]. The weights corresponded to the number of data available in a given year/region/season. The slope of the linear regression of the annual mean property was used to describe the trend; a total of 40 trends were computed (eight datasets × five properties).

3 Results

3.1. [Chl-a], [Fucox], absorption coefficients, and *PAAW* seasonal and regional variations

For the three biogeochemical regions, both mean [Chl-a] and [Fucox] were highest in spring when phytoplankton bloom and the community assemblage is dominated by diatoms (Figure 2). Mean values of 2.70, 1.80, and 2.73 mg m^{-3} were recorded for [Chl-a] on the Scotian Shelf, NAB, and the Labrador Sea, respectively, and mean values of 0.89, 0.47, and 0.72 mg m^{-3} were recorded for [Fucox] on the Scotian Shelf, NAB, and the Labrador Sea, respectively (Table 1). The Scotian Shelf showed the highest seasonal variability with a strong decrease of both [Chl-a] and [Fucox] in summer followed by an increase during autumn and a second decrease in winter for [Chl-a], which remained higher than the mean summer values, while [Fucox] in winter was greater than in autumn (Table 1). Both [Chl-a] and [Fucox] in NAB followed the same seasonal pattern as the one on the Scotian Shelf, but with smaller mean values. The Labrador Sea exhibited a different seasonal cycles than the two other regions, as both [Chl-a] and [Fucox] continuously decreased from summer to winter when it reached the lowest values of all regions and seasons (i.e., [Chl-a] = 0.19 mg m^{-3} and [Fucox] = 0.05 mg m^{-3}). The similar seasonal cycle between [Chl-a] and [Fucox] is supported by the high degree of correlation between the two pigments (R^2 = 0.85, Figure 3).

As for [Chl-a] and [Fucox], the absorption coefficients at 443 nm for non-algal particles and phytoplankton spanned about three orders of magnitude and followed a normal distribution when $\log_{10}$-transformed (Supplementary Figure S2). All properties showed large regional and seasonal variabilities (Table 1 and Figure 2). Data revealed the same seasonal cycle for a_ϕ(443) as for [Chl-a] with the exception that a_ϕ(443) was slightly higher in autumn (0.059 m^{-1}) than in spring (0.050 m^{-1}) on the Scotian Shelf (Table 1). The absorption coefficient at 675 nm (Figure 2B) exhibited the same seasonal cycle as a_ϕ (443) with smaller values as expected (Figures 2A, B). The specific absorption coefficient at 443 nm a^*_ϕ(443) in mg Chl-a m^{-2} (Figure 2C) showed an inverse pattern to [Chl-a] and a_ϕ(443) in all regions, perhaps with less variability between summer and autumn on the Scotian Shelf compared to a_ϕ(443) and the notable exception of the low mean a^*_ϕ(443) in the Labrador Sea when [Chl-a] is also low. The absorption coefficient at 443 nm by non-algal particulate matter exhibited a different seasonal pattern than a_ϕ(443) on the Scotian Shelf, with high values reached in the spring followed by a decrease in summer with an increase for both autumn and winter (Figure 2D). In the NAB, a_{NAP} (443) was highest in spring, with values relatively low (0.0051 m^{-1}) compared to the Scotian Shelf (0.009 m^{-1}) and Labrador Sea (0.0075 m^{-1}). For the rest of the year, a_{NAP} (443) remained quasi constant with values of about 0.0035 m^{-1} (ANOVA test p-value < 0.05). In the Labrador Sea, a_{NAP} (443) showed a similar seasonal pattern to a_ϕ(443) with a continuous decrease from spring to winter, unlike the two other regions where markedly different seasonal patterns were observed. The slope of the *NAP* absorption spectrum also shows very weak seasonal dependence (Figure 2E), with a slight decrease from spring to winter on both the Scotian Shelf and NAB, while S_{NAP} reaches a maximum in autumn in the Labrador Sea.

The *PAAW* provided additional information to [Chl-a], a_ϕ (443), and a^*_ϕ(443) (Figure 2F). The overall *PAAW* for the Northwest Atlantic was 478 nm (Table 1). On the Scotian Shelf, *PAAW* exhibited a seasonal cycle that resembled the one of a^*_ϕ (443) with a mean value of 482.5 nm in spring that decreased to 470.2 nm in summer to increase again in autumn (477.5 nm) and winter (480.9 nm). The spring season on the Scotian Shelf exhibited the highest range of variation in *PAAW* of all regions/seasons with about 40 nm in variation from 461.6 to

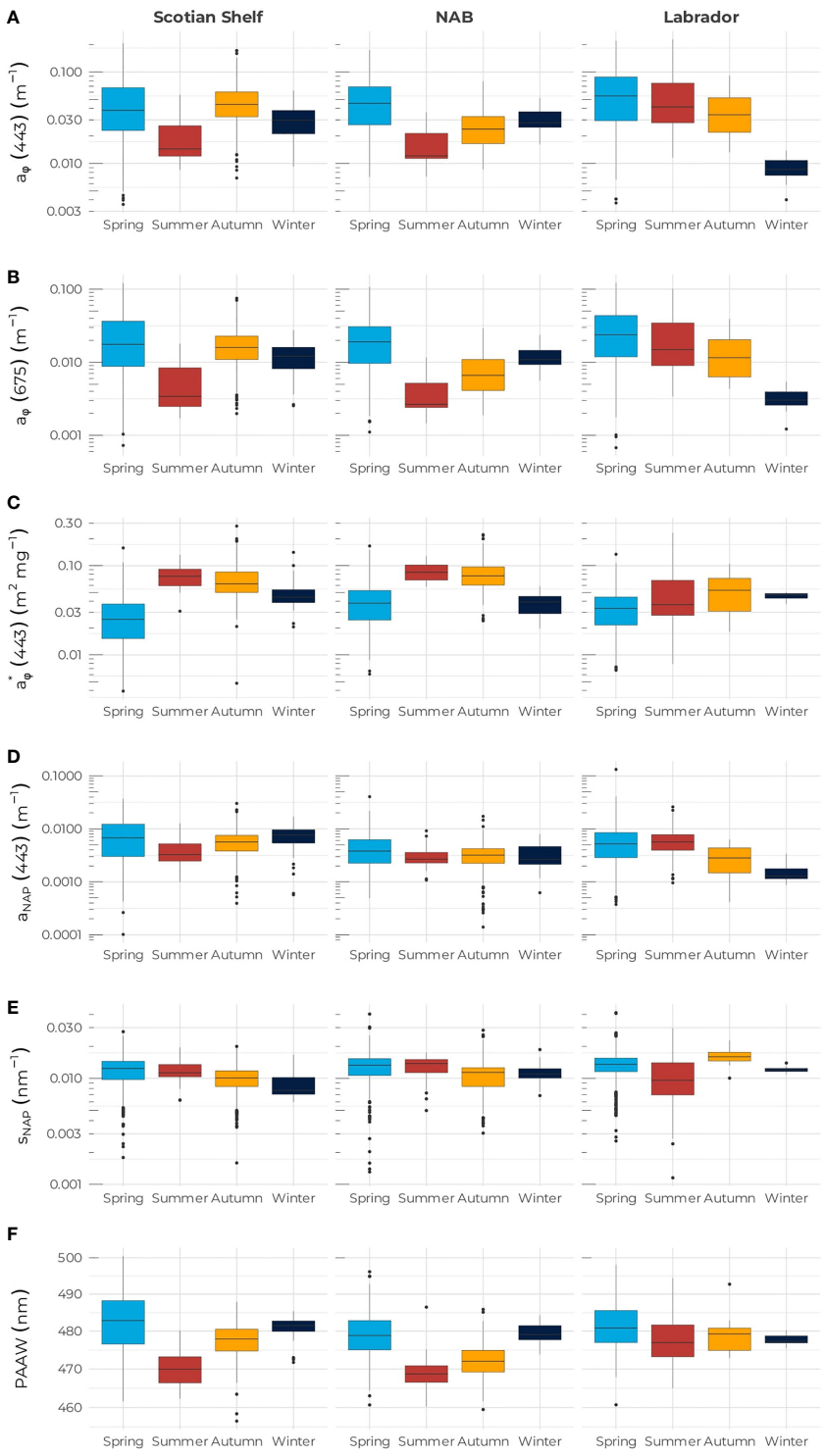

FIGURE 2
Mean and one standard deviation (i.e., boxplot) of **(A)** $a_\phi(443)$ **(B)** $a_\phi(675)$, **(C)** $a^*_\phi(443)$, **(D)** a_{NAP} (443), **(E)** S_{NAP}, and **(F)** *PAAW* for the Scotian Shelf (left column), Northwest Atlantic Basin (middle column), and Labrador Sea (right column). In each panel, the blue, red, yellow, and black boxes correspond to spring, summer, autumn, and winter, respectively.

TABLE 1 Mean values and range of variations (min–max) of [Chl-a], [Fucox], $a_\phi(443)$, $a_\phi^*(443)$, a_{NAP} (443), S_{NAP} and *PAAW* for the Scotian Shelf, Northwest Atlantic, and Labrador Sea in spring, summer, autumn, and winter.

Season	*N*	[Chl-a]	[Fuco]	a_ϕ (443)	$a_\phi^*(443)$	a_{NAP} (443)	S_{NAP}	*PAAW*
All data	2,267	1.53	0.41	0.048	0.055	0.0065	0.0115	478.5
		(0.06–17.5)	(0–6.68)	(0.004–0.231)	(0.004–0.290)	(0.0002–0.1384)	(0.0001–0.0415)	(456.5–500.5)
Scotian Shelf								
Spring	781	2.70	0.89	0.049	0.0297	0.009	0.0124	482.5
		(0.102–13.6)	(0.000–6.68)	(0.004–0.216)	(0.004–0.1636)	(0.0002–0.0378)	(0.0018–0.0275)	(461.6–500.5)
Summer	36	0.32	0.03	0.022	0.0781	0.0042	0.0118	470.2
		(0.093–0.882)	(0.000–0.131)	(0.009–0.057)	(0.0321–0.133)	(0.001–0.0132)	(0.0062–0.0195)	(462.3–480.1)
Autumn	781	0.83	0.13	0.050	0.0724	0.0065	0.01	477.5
		(0.080–4.13)	(0.000–1.68)	(0.007–0.177)	(0.0048–0.2896)	(0.0004–0.0314)	(0.0004–0.02)	(456.5–487.9)
Winter	74	0.68	0.16	0.032	0.0493	0.0078	0.0088	480.9
		(0.211–1.59)	(0.053–0.517)	(0.009–0.064)	(0.0212–0.1463)	(0.0007–0.0178)	(0.006–0.0167)	(471.7–485.4)
Northwest Atlantic Basin								
Spring	313	1.80	0.47	0.051	0.0421	0.0051	0.0131	479.0
		(0.091–10.4)	(0.000–5.37)	(0.008–0.176)	(0.0063–0.1724)	(0.0005–0.0419)	(0.0001–0.0403)	(460.7–496.1)
Summer	58	0.21	0.03	0.017	0.0890	0.0033	0.0129	469.1
		(0.090–0.553)	(0.000–0.168)	(0.007–0.037)	(0.0598–0.1373)	(0.0009–0.0095)	(0.005–0.0175)	(460.2–486.5)
Autumn	369	0.400	0.040	0.028	0.0838	0.0036	0.011	472.1
		(0.060–2.19)	(0.000–0.892)	(0.009–0.081)	(0.0246–0.2305)	(0.0002–0.0184)	(0.003–0.0284)	(459.5–485.8)
Winter	45	0.87	0.16	0.032	0.0389	0.0037	0.0111	479.4
		(0.531–2.03)	(0.031–0.796)	(0.016–0.054)	(0.0204–0.0607)	(0.0006–0.0082)	(0.0069–0.0186)	(473.8–484.3)
Labrador Sea								
Spring	504	2.73	0.72	0.063	0.0363	0.0075	0.0134	481.5
		(0.076–17.5)	(0.000–4.73)	(0.004–0.224)	(0.0069–0.1428)	(0.0004–0.1384)	(0.0026–0.0415)	(460.7-498.1)
Summer	275	1.99	0.67	0.061	0.0489	0.0068	0.0106	477.7
		(0.10–8.48)	(0.000–4.43)	(0.012–0.231)	(0.0081–0.2402)	(0.0011–0.0289)	(0.0012–0.0297)	(465.0–494.4)
Autumn	24	0.88	0.26	0.038	0.0538	0.0031	0.0163	478.7
		(0.225–3.19)	(0.000–1.41)	(0.014–0.093)	(0.0188–0.1069)	(0.0004–0.0065)	(0.01–0.0228)	(472.9–492.7)
Winter	19	0.19	0.05	0.009	0.0471	0.0017	0.0121	477.8
		(0.093–0.321)	(0.017–0.155)	(0.004–0.014)	(0.0377–0.0521)	(0.001–0.0037)	(0.0109–0.0139)	(475.4–480.2)

Note that ***N*** corresponds to the number of samples collected, and the actual number of a given property might be lower after quality control or due to mishandling during data processing.

500 nm. In the NAB, *PAAW* followed a similar pattern to a_ϕ (443) and $a_\phi(675)$; *PAAW* in all seasons was smaller than the *PAAW* observed on the Scotian Shelf. Interestingly, the *PAAW* in the Labrador Sea showed a different pattern than the $a_\phi^*(443)$ and a_ϕ (443) ones, associated with the lowest seasonal variability (477.7 nm in summer to 481.5 nm in spring). The *PAAW* was highest in spring and lowest in winter, while summer and autumn exhibited similar values.

3.2. Bio-optical relationships: [Chl-a], [Fucox], $a_\phi(443)$, $a_{NAP}(443)$ and S_{NAP}

The [Chl-a]: $a_\phi(\lambda)$ relationship is arguably the most studied of all the bio-optical properties. When grouping all the data together, independently of regions and seasons, the linear regression of a_ϕ (443) against [Chl-a] in the $\log_{10}$ space can be described in the linear space as:

$$a_\phi(443) = 0.0407[\text{Chl-a}]^{0.515} \quad (3)$$

The regional relationships exhibited a large difference in the exponent with values of 0.469, 0.508, and 0.616 for the Scotian Shelf, NAB, and the Labrador Sea, respectively, while the intercept in the $\log_{10}$ space remained similar and varied between −1.37 and −1.42 (corresponding to 0.038 to 0.042 in the linear space) for the three regions (Figure 4B). The Scotian Shelf showed the lowest R^2, with a value of 0.53 that may be driven by seasonal variations. As for the [Chl-a]– $a_\phi(443)$ relationship, the $a_{NAP}(443)$:$a_\phi(443)$ relationship showed regional differences in all three regions, but with $a_\phi(443)$ dominating systematically the particulate absorption (Figure 5). High variability around the model was consistent with low correlation coefficients, in particular on the Scotian Shelf and NAB. The slope of the linear regression of a_{NAP} (443) against a_ϕ (443) was 0.73 (R^2 = 0.35), 0.59 (R^2 = 0.27), and 0.66 (R^2 = 0.41) for the Scotian Shelf, NAB, and Labrador Sea, respectively.

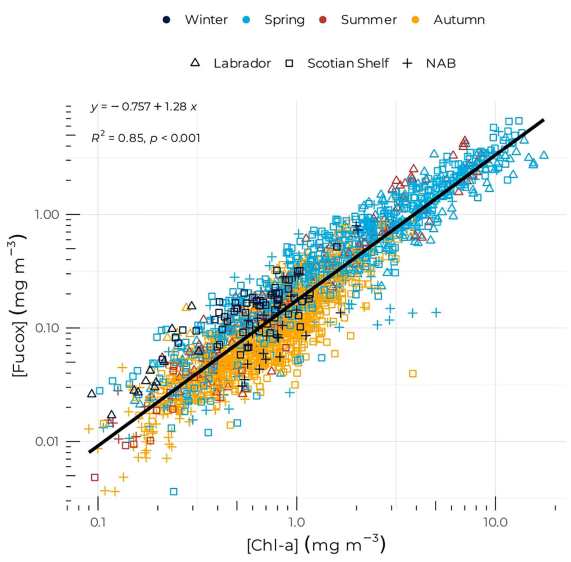

FIGURE 3
[Fucox] as a function of [Chl-a]. Symbols are color-coded according to season as in Figure 2.

3.3. Spectral variation in phytoplankton absorption

At the Northwest Atlantic scale, both [Chl-a] and [Fucox] were highly correlated to $a_\phi(443)$:$a_\phi(675)$ with R^2 of 0.73 and 0.77, respectively (Figures 6A and S3). The slope of the regression was lower in the Labrador Sea (i.e., 0.165) compared to the other two bio-regions (0.219 and 0.231 for the Scotian Shelf and NAB respectively, Figure 6B). [Chl-a] was slightly more correlated with a_ϕ (675) ($R^2 = 0.89$) compared to a_ϕ (443) ($R^2 = 0.81$), hinting that other pigments might contribute to absorption in the blue part of the absorption spectrum.

The *PAAW* showed that the spectral shape of the phytoplankton absorption varied across the three bio-regions (Figure 7). For the three regions, a large *PAAW* corresponds to normalized spectra with the flattest shape, where the difference between the blue and red absorption peak is the smallest (Figure 7A). As phytoplankton in the blue part of the spectrum increases and a shoulder occurs around 490 nm, the *PAAW* decreases. The Scotian Shelf showed the highest variability in *PAAW* with some of the "brownest" phytoplankton with *PAAW* as high as 500 nm (Figure 7B). The distribution of *PAAW* on the Scotian Shelf shows a bimodal shape centered on about 482 nm with a second small bump located around 492 nm, likely the contribution from the spring samples. The *PAAW* in the NAB region followed a normal distribution, which was centered on 476 nm and corresponded to the smallest mean *PAAW* of the three regions. Finally, the Labrador Sea region exhibited the narrowest range of variation for the *PAAW* index, with a mean value and distribution similar to the Scotian Shelf. PAAW was positively correlated to [Chl-a] and negatively correlated to $a^*_\phi(443)$ (Figures 8A, B). A second-order polynomial equation was used to model the decrease of the $a_\phi(443)$:$a_\phi(675)$ ratio with increasing *PAAW* (Figure 8C). High values of *PAAW* were associated with low values of the ratio in the spring. A high spread in the data occurred at low *PAAW* (Figure 8C). The variance in [Chl-a] was slightly better explained by *PAAW* ($R^2 = 0.69$) than by $a_\phi(443)$ (Figure 4B, $R^2 = 0.65$). Using *PAAW* to predict the $a_\phi(443)$:$a_\phi(675)$ ratio compared to [Chl-a] increased R^2 from 0.72 to 0.87 (Figures 6, 8C). The *PAAW* seasonal cycles in all three regions exhibited opposite seasonal cycles compared to that of $a_\phi(443)$:$a_\phi(675)$ (Supplementary Figure S4).

3.4. Trend analysis of *PAAW*, and phytoplankton and NAP absorption

Trend analysis of the *PAAW* for the entire dataset and all regions did not show any significant changes; all the trends were positive but with *p*-values that remained high. However, trend analysis at both the regional and seasonal levels revealed a significant increase in the *PAAW* in all three regions in spring (Table 2 and Figure 9). The Scotian Shelf exhibited the highest rate of change with a slope of 0.38 nm year^{-1} followed by the Labrador Sea (0.35 nm year^{-1}) and the NAB (0.23 nm year^{-1}). The autumn showed an opposite trend: a decrease in the *PAAW* on both the Scotian Shelf (−0.15 nm year^{-1}) and the NAB (−0.35 nm year^{-1}). [Chl-a] showed a significant negative trend in autumn on both the Scotian Shelf and NAB, with trends of −0.017 and −0.028 mg m^{-3} year^{-3} (Table 2 and Supplementary Figure S5). Phytoplankton absorption at 443 nm showed a significant negative trends at the 0.01 level only in the NAB region in autumn ($-0.15e^{-4}$ m^{-1} year^{-1}) and at the 0.1 level on the Scotian Shelf also in autumn (Table 2 and Supplementary Figure S6).

For the non-algal particles, the magnitude [i.e., a_{NAP} (443)] exhibited changes at the entire scale of the Northwest Atlantic and in both the Scotian Shelf and NAB regions (Table 2 and Supplementary Figure S7) with positive and significant trends that ranged between $1e^{-4}$ and $2e^{-4}$ m^{-1} year^{-1}. At the seasonal level, only the Scotian Shelf and NAB in spring showed positive significant trends of $4.1e^{-4}$ and $2.2e^{-4}$ m^{-1} year^{-1}, respectively. The annual slope of the $a_{NAP}(443)$:$a_\phi(443)$ time series was positive and significant for all datasets except for the Labrador Sea in spring and the NAB in autumn (Table 2 and Supplementary Figure S8). The highest trend was observed on the Scotian Shelf in spring (slope: $6.9e^{-3}$ m^{-1} year^{-1}) and the lowest trend was observed also on the Scotian Shelf but in autumn (slope: 6.9 e^{-3} m^{-1} year^{-1}).

Our long time series also provided the opportunity to test the number of data required to characterize the variability of the ecosystems by examining the mean and standard deviation (SD) of [Chl-a], $a_\phi(443)$, and $a_{NAP}(443)$ as a function of time for cumulative measurements (Figure 10). The assumption was that the variability of the ecosystem was described when the mean

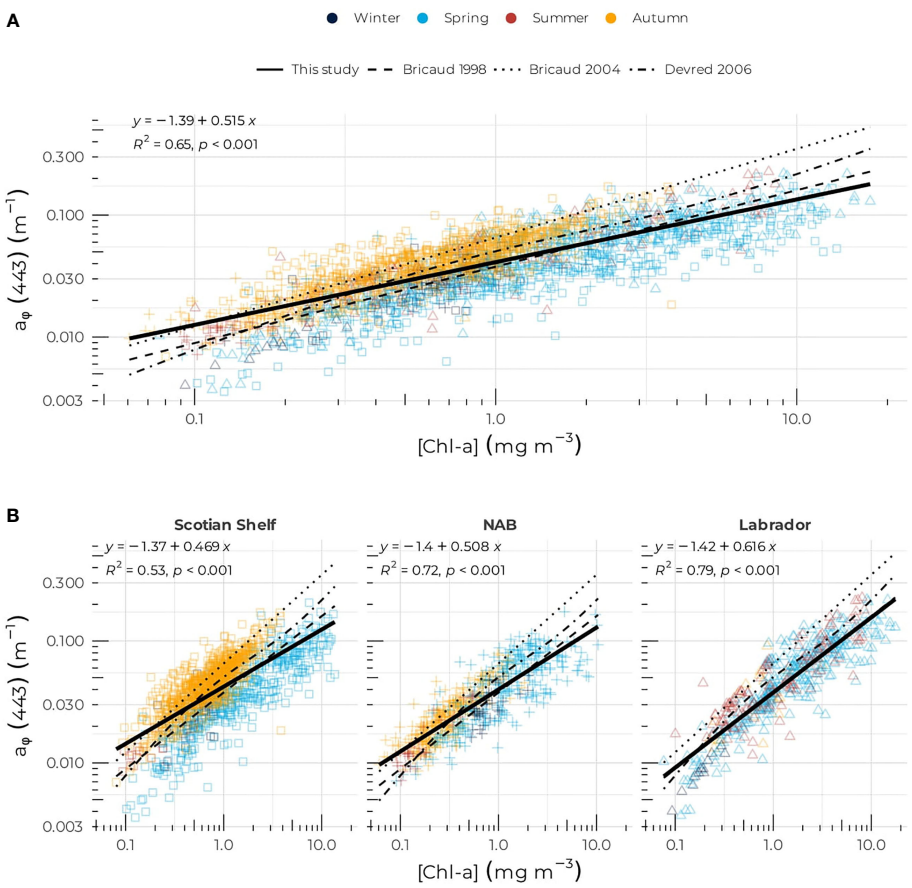

FIGURE 4
Phytoplankton absorption coefficient at 443 nm, $a_\phi(443)$, as a function of [Chl-a] for **(A)** the entire dataset, **(B)** the Scotian Shelf (left panel), the Northwest Atlantic Basin (rmiddle panel), and the Labrador Sea (right panel). The solid black lines correspond to the power law fit (Equation 3); the long-dashed, short-dashed, and dotted-dashed lines correspond to Broca's et al. (1998), Bricaud (2004), and Devred et al. (2006), models respectively. Symbols are color-coded according to season as in Figure 2.

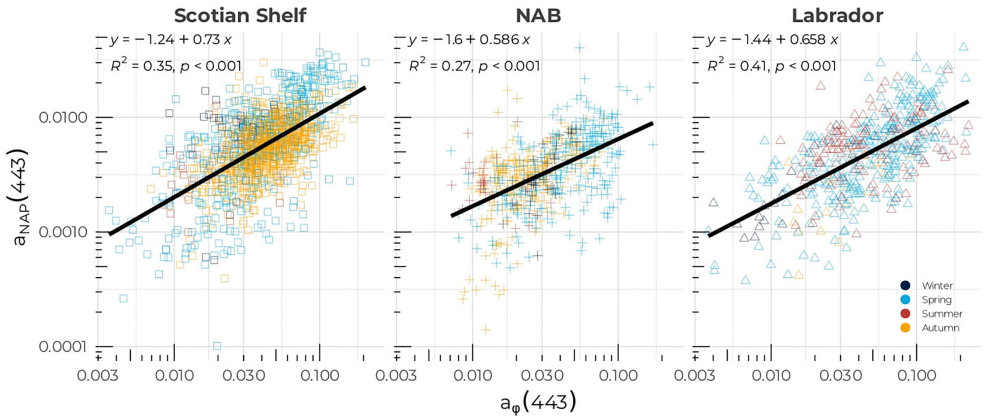

FIGURE 5
Non-algal particulate absorption coefficient at 443 nm, a_{NAP} (443), as a function of $a_\phi(443)$ for the Scotian Shelf (left panel), the Northwest Atlantic Basin (middle panel), and the Labrador Sea (right panel). The solid black lines correspond to the linear regression of a_{NAP} (443) versus a_ϕ (443). Symbols are color-coded according to season as in Figure 2.

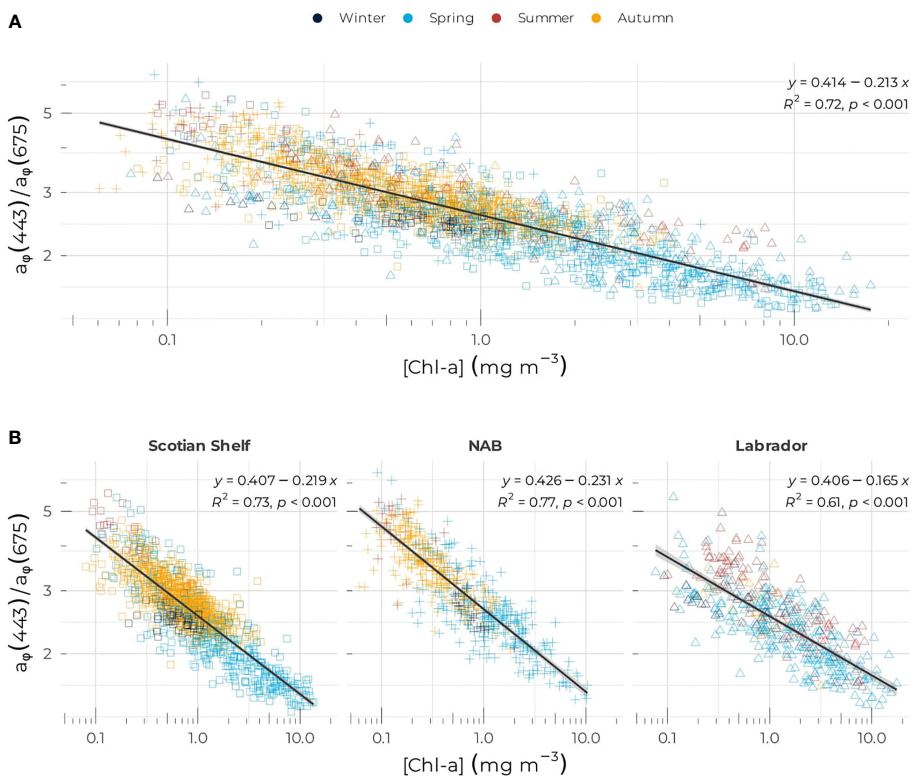

FIGURE 6
Ratio of a_ϕ (443) to a_ϕ (675) as a function of [Chl-a] for **(A)** the entire dataset and **(B)** the Scotian Shelf (left panel), the Northwest Atlantic Basin (middle panel), and the Labrador Sea (right panel). Symbols are color-coded according to season as in Figure 2.

and SD reach an asymptotic value. The standard deviations of [Chl-a] and a_ϕ(443) reached their asymptotic values after 10 years of sampling (about 650 measurements) in spring. After 20 years of data collection, [Chl-a] and a_ϕ(443) standard deviations did not stabilize in summer nor autumn, suggesting that the Scotian Shelf is still undergoing significant changes during these two seasons and continuous sampling is required to fully characterize the bio-optical dynamics of the Scotian Shelf. About 250 (150) points collected over 5 years of sampling in spring (summer) and about 550 points collected over 10 years in autumn on the Scotian Shelf were sufficient to capture the variability in a_{NAP} (443).

4 Discussion

In the current study, we have used an extensive dataset of several bio-optical parameters to examine their variability and linkage in the Northwest Atlantic. In general, our results agreed, and reinforced, current knowledge about variation in phytoplankton biomass and community structure associated with changes in phytoplankton and non-algal particulate absorption. The added value of our current study relies upon the quantification of the spatiotemporal variations in bio-optical properties in the Northwest Atlantic, as well as the definition of an index to summarize phytoplankton absorption over 400 to 700 nm in a single number: *PAAW*. Most studies rely on data from a single cruise (e.g., Stuart et al., 2000; Pérez et al., 2021), a combination of cruises gathered from one region (Ferreira et al., 2013; Matsuoka et al., 2014) or the global ocean without a pre-defined temporal strategy (Trees et al., 2000; Ciotti et al., 2002; Bricaud et al., 2004; Brewin et al., 2011). The DFO monitoring cruises have systematically carried out measurements of bio-optical properties at about 150 fixed stations spanning about 20° in latitudes (i.e., 42 to 62°N) in the NWA and covering the entire seasonal cycle for more than 20 years. The NWA was divided into three regions with markedly different regimes: (1) The Scotian Shelf showed a regime of a mid-latitude shelf environment, with high seasonal variations in phytoplankton biomass and associated properties; (2) the NAB showed dynamics of an oligotrophic environment, with low biomass compared to the two other regions and a more subtle seasonal cycle; and, finally, (3) the Labrador Sea exhibited the characteristics of a sub-arctic environment with a delayed spring growth in phytoplankton biomass (Wu et al., 2008) and the absence of an autumn bloom.

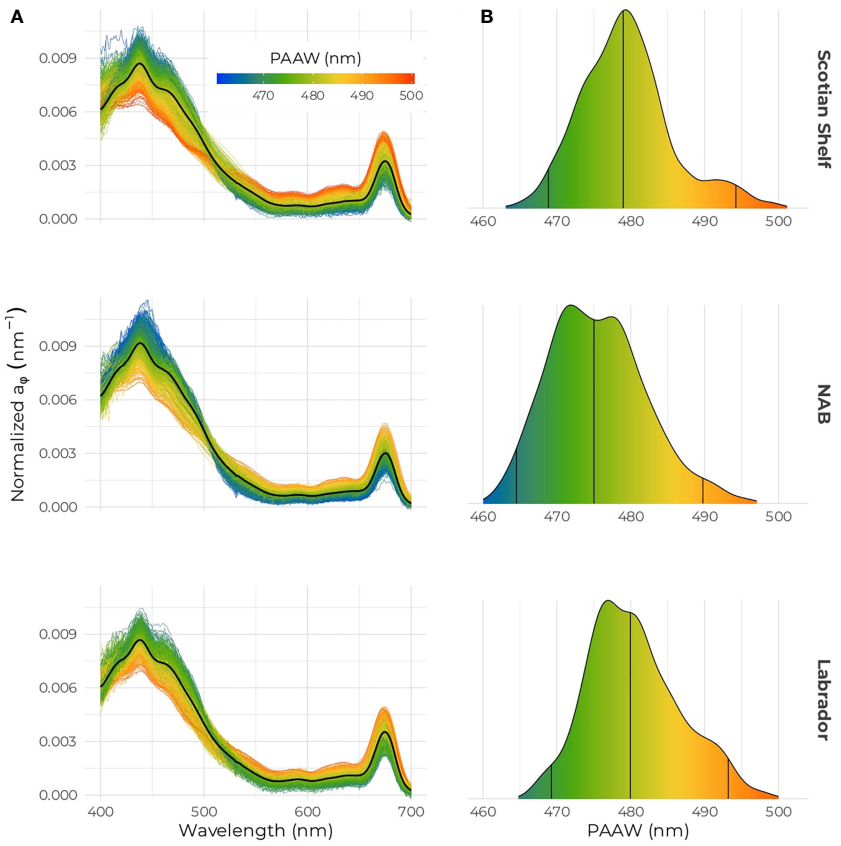

FIGURE 7
(A) Phytoplankton absorption spectra and **(B)** distribution of the *PAAW* for the Scotian Shelf (top), NAB (middle) and the Labrador Sea (bottom); the color bar indicates the *PAAW* values in all panels.

4.1. Phytoplankton biomass and absorption in the Northwest Atlantic

The coefficients of the power law that expressed a_ϕ (443) as a function of [Chl-a] (Eq. 3) found in the current study were consistent with coefficients computed in previous studies. The coefficients found here were close to the ones found by Bricaud et al. (1998) (Figure 4A) who reported a factor of 0.0378, but with a smaller exponent (Bricaud et al., 1998, i.e., 0.627). Bricaud et al. (2004) found a factor of 0.0654 and an exponent of 0.728, which are higher than the ones found here. The coefficients in this study were also consistent with the one found by Devred et al. (2006), which were computed using some of the data included in the current study. In general, all models agreed well in the bulk range of [Chl-a] between 0.3 and 5 mg m^{-3} and discrepancies between models occurred mainly in the extreme range of values and can be attributed to the type of waters sampled. For instance, the oligotrophic waters sampled by Bricaud et al. (2004) explained the higher coefficients compared to this study. This is also highlighted in the regional differences that we found between the three regions of the Northwest Atlantic as emphasized by Stuart et al. (2000) who showed that diatom-dominated waters of the Labrador Sea exhibited a lower absorption coefficient per unit of [Chl-a] than waters dominated by prymniesophytes. This finding led to the development of a satellite-based algorithm to derive the probability of diatom occurrence in the Northwest Atlantic (Sathyendranath et al., 2004). Seasonal changes in solar radiation, temperature, and nutrient availability are among the main drivers that regulate the size structure, the intracellular pigment composition, and the absorption characteristics of the algal populations (Ciotti et al., 1999; Ciotti et al., 2002; Bricaud et al., 2004; Churilova et al., 2017). The spring bloom in the NWA is dominated by diatoms in all three regions as suggested by the low phytoplankton specific absorption coefficient and high [Fucox] observed during that time (Table 2), in agreement with phytoplankton enumeration carried out at a fixed station on the Scotian Shelf (Casault et al., 2020) and other studies (Trzcinski et al., 2013; Fragoso et al., 2017; Zang et al., 2022). The higher the fucoxanthin concentration, suggesting a high diatom

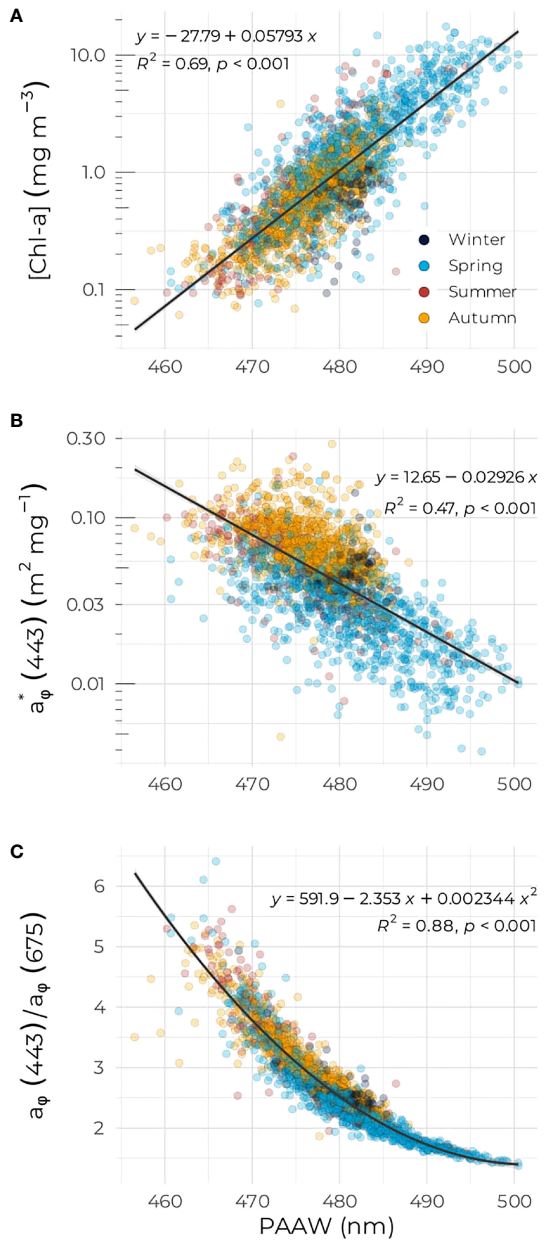

FIGURE 8
(A) [Chl-a], **(B)** $a^*_\phi(443)$, and **(C)** $a_\phi(443)$:$a_\phi(675)$ as a function of *PAAW* for the entire dataset.

biomass, the lower the phytoplankton-specific absorption in spring (Table 2), with the Scotian Shelf showing the highest abundance of diatoms, followed by the Labrador Sea and the NAB. The autumn bloom on the Scotian Shelf and in the NAB exhibited $a^*_\phi(443)$ that were much higher than during spring, despite relatively high phytoplankton biomass, suggesting that large phytoplankton other than diatoms (e.g., dinoflagellates) dominated the phytoplankton assemblage and were associated with low packaging effect (Figure 2C and Table 1). Species succession in the Labrador Sea showed a different pattern than the Scotian Shelf and NAB with a continuous decrease (increase) of phytoplankton biomass ($a^*_\phi(443)$). While high biomass and dominance of diatoms have been established in spring in the Labrador Sea using both phytoplankton counts and pigment composition (Fragoso et al., 2017; Fragoso et al., 2018), this study reveals for the first time the entire annual cycle of phytoplankton assemblages based on optical traits with large cells dominating the spring and summer signal while small cells dominated the optical signal in autumn. The low biomass in winter, associated with relatively high [Fucox] and $a^*_\phi(443)$, suggests that phytoplankton are adapted to a low-light environment. Although no direct measurements of the phytoplankton cell size were made during the DFO oceanographic cruises, a rich literature has demonstrated that inferences of cell size could be made from IOPs. For instance, results from Fujiki and Tagushi (2002) indicated that a decrease in a_ϕ (675) was solely associated with increasing phytoplankton cell volume and packaging effect. Likewise, Bricaud et al. (1995) found that an increase in [Chl-a] was negatively correlated with both $a^*_\phi(443)$ and the blue-to-red phytoplankton absorption ratio (see Figure 8C), which was attributed to an increase in pigment packaging and low concentration of accessory pigments (Staehr et al., 2004; Vishnu et al., 2018). Here, we found a decrease of the $a_\phi(443)$:$a_\phi(675)$ ratio with [Fucox] for the entire dataset with a slope of −0.163 (Supplementary Figure S3) in the $\log_{10}$-space (0.23 in the linear space), which is consistent with the results of Hoepffner and Sathyendranath (1993) who found an increase of $a_\phi(440)$:$a_\phi(550)$ with [Fucox] from 0.05 to 0.3 depending on the phytoplankton assemblage. While Hoepffner and Sathyendranath (1993) used a different phytoplankton absorption ratio compared to this study, their results point in the same direction of change in phytoplankton spectral shape with change in diatom biomass.

Spatiotemporal variations of non-algal particulate absorption magnitude and spectral dependence showed complex patterns (Figures 2D, E). The dataset encompassed a wide range of variations in both a_{NAP} (443) and S_{NAP} driven by seasonality and the type of water sampled. However, several patterns emerged at the regional scale, $a_{NAP}(443)$ remained below 11% of $a_\phi(443)$ on average, with the highest $a_{NAP}(443)$: $a_\phi(675)$ ratio observed in the mesotrophic environment of the Scotian Shelf and the lowest values occurring in the NAB (Table 1). Large discrepancies were observed around the mean relationship (Figure 5), suggesting that many short-term processes may be included in the production of detritus from living phytoplankton (i.e., grazing and viral lysis). However, only a study at high temporal frequency sampling (i.e., several times a day for several days) may reveal the processes involved in the degradation of phytoplankton and lead to a detailed understanding of the

TABLE 2 Slope, p-value (NS: non-significant) and correlation coefficient (R^2) of the linear regression of *PAAW* (in nm year^{-1}), [Chl-a] (in mg m^{-3} year^{-1}), a_ϕ (443) (in m^{-1} year^{-1}), a_{NAP} (443) (in m^{-1} year^{-1}) and a_{NAP} (443) : a_ϕ (443) (in year^{-1}) against time in year.

Dataset	*PAAW*			[Chl-a]			a_ϕ (443)			A_{NAP} (443)			A_{NAP} (443) : a_ϕ (443)		
	Slope	*p*-value	R^2	Slope	*p*-value	R^2	Slope	*p*-value	R^2	Slope	*p*-value	R^2			
All	0.083	NS	0.11	-8.7e^{-3}	NS	0.01	-1.1 e^{-4}	NS	0.01	1.8 e^{-3}	<0.01	0.41	4.4 e^{-3}	<0.01	0.01
Regions															
Scotian Shelf	0.107	NS	0.05	−0.010	NS	0.01	−1.2 e^{-4}	NS	0.01	2.0 e^{-4}	<0.01	0.32	4.7 e^{-3}	<0.01	0.40
NAB	0.136	NS	0.10	−0.013	NS	0.02	−1.4 e^{-5}	NS	0.01	1.0 e^{-4}	<0.05	0.23	3.0 e^{-3}	<0.05	0.26
Labrador Sea	0.082	NS	0.08	−0.085	NS	0.07	−1.1 e^{-3}	NS	0.07	1.4 e^{-3}	NS	0.26	4.9 e^{-3}	<0.05	0.26
Regions in Spring															
Scotian Shelf	0.382	<0.05	0.28	−0.063	NS	0.04	6 e^{-4}	NS	0.05	4.1 e^{-4}	<0.05	0.37	6.9 e^{-3}	<0.01	0.39
NAB	0.229	<0.05	0.36	−0.032	NS	0.06	5 e^{-4}	NS	0.04	2.2 e^{-4}	<0.05	0.41	3.8 e^{-3}	<0.1	0.34
Labrador Sea	0.347	<0.05	0.32	−0.026	NS	0.01	15 e^{-4}	NS	0.08	0.3 e^{-4}	NS	0.01	3.4 e^{-3}	NS	0.10
Regions in Autumn															
Scotian Shelf	−0.155	<0.05	0.27	−0.017	<0.01	0.36	−5.2 e^{-4}	<0.1	0.17	0.4 e^{-4}	NS	0.04	2.4 e^{-3}	<0.05	0.26
NAB	−0.348	<0.05	0.61	−0.018	<0.01	0.68	−15 e^{-4}	<0.01	0.80	0.6 e^{-4}	NS	0.10	4.8 e^{-3}	NS	0.24

absorption dynamics of phytoplankton and non-algal particles. Diatom-dominated phytoplankton biomass, as indicated by [Fucox], was associated with high a_{NAP} (443) and high S_{NAP} (Table 1). For instance, relatively high [Chl-a] and [Fucox] on the Scotian Shelf (2.7 and 0.89 mg m^{-3}, respectively) and Labrador Sea (2.7 and 0.72 mg m^{-3}, respectively) in spring were associated with high a_{NAP} (443) (0.009 and 0.0075 m^{-1} for the Scotian Shelf and Labrador Sea, respectively) and S_{NAP} (0.0124 and 0.0134 m^{-1} for the Scotian Shelf and Labrador Sea, respectively). On the other hand, low [Chl-a] and [Fucox] in the NAB in summer were

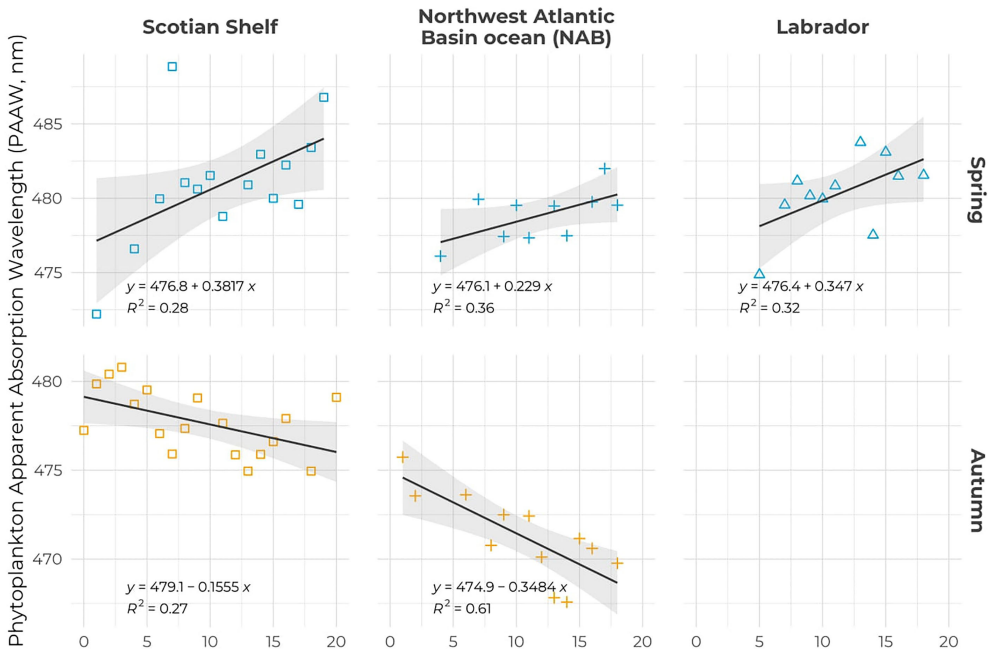

FIGURE 9
Seasonal trends in *PAAW* for spring (top panels) and autumn (bottom panels) for the Scotian Shelf (left), NAB (middle), and the Labrador Sea (right). The black solid lines correspond to the linear regression of *PAAW* against time with the coefficient and R^2 indicated in each panel. Symbols are color-coded according to season as in Figure 2.

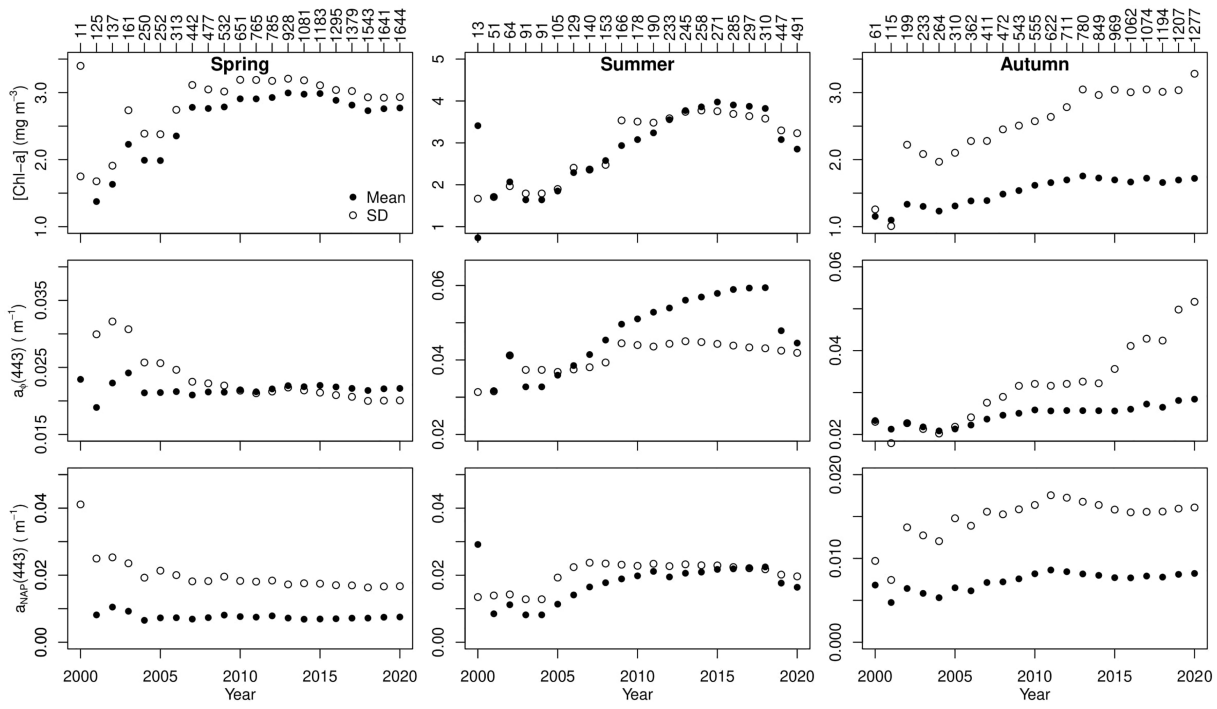

FIGURE 10
Mean (solid black circles) and standard deviation (open black circles) as a function of time for [Chl-a] (top), a_ϕ (443) (middle), and a_{NAP} (443) (bottom) (you should use text mode to write NAP instead of math mode; it does not look good) in spring (left column), summer (middle column), and autumn (right column on the Scotian Shelf.

associated with low $a_{NAP}(443)$ and S_{NAP}. A departure from this pattern was the high [Chl-a] and low [Fucox] associated with relatively low a_{NAP} (443) and S_{NAP} on the Scotian Shelf in autumn. Magnitude and spectral absorption by detritus may depend on the phytoplankton assemblage and growth state, and its degradation through biogeochemical processes (e.g., virus infection, Nagasaki, 2008). The spring bloom also corresponds to the maximum of zooplankton abundance on the Scotian Shelf (Casault et al., 2020) and a number of studies have demonstrated the selective feeding of zooplankton on diatoms (Teegarden et al., 2001; Leising et al., 2005). Grazing by zooplankton results in the production of phaeopigments (Shuman and Lorenzen, 1975; Head and Horne, 1993; Collos et al., 2005) and increases the concentration of detritus (i.e., non-algal particles) in the water column and therefore its absorption in agreement with the highest relative absorption of non-algal particles measured in spring and autumn during bloom conditions. These processes suggest that the spectral slope of the absorption by *NAP* might be impacted by community structure and zooplankton grazing; however, this statement would need to be further studied. Our results, however, support that zooplankton grazing may impact the bulk optical properties of seawater. The emergence of new sensors with hyperspectral capability may help inform secondary production using variation in a_{NAP} as an indicator of zooplankton grazing activity.

4.2. The phytoplankton apparent absorption wavelength: An integrative index of the spectral shape of phytoplankton absorption

Spectral variation in phytoplankton absorption, as indicated by the $a_\phi(443)$:$a_\phi(675)$ ratio, as a function of [Chl-a] provides a rapid assessment of the packaging effect and therefore a rough estimation of community structure (Bricaud et al., 2004; Devred et al., 2006; Vishnu et al., 2018). In addition, retrieval of pigment concentration from absorption spectra has been carried out in the past using gaussian decomposition (Hoepffner and Sathyendranath, 1991; Chase et al., 2013; Zhang et al., 2021), machine learning (Chazottes et al., 2006; Bricaud et al., 2007), and derivative analysis (Bidigare et al., 1989; Catlett and Siegel, 2018) to cite a few methods. Here, we use an integrative index and relate it to phytoplankton bio-optical properties. The takeaway message from this index is that it performs slightly better, in terms of R^2, than any other variable, namely, [Chl-a], [Fucox], $a_\phi(443)$, and a_ϕ

(443):a_ϕ(675) when studying the triangular relationship between absorption, biomass, and community structure. The *PAAW* provides information on the trophic status as supported by the high correlation coefficient with [Chl-a] (R^2 = 0.69), which was similar to the [Chl-a]– a_ϕ (443) one (R^2 = 0.65). The other advantage of the *PAAW* is that it can also be used to describe the community structure given its high correlation to a_ϕ(443):a_ϕ(675) (R^2 = 0.88) and [Fucox] (R^2 = 0.69, result not shown). Analysis of the phytoplankton absorption spectral variation showed consistency with *PAAW* and, notably, non-linear changes in the absorption spectra from small cell to large cell that translated into an increase in *PAAW* (Figure 8C). Another advantage of the *PAAW* is that its variation on a linear scale, compared to other bio-optical parameters that are expressed on a $\log_{10}$ scale, makes it a valuable index to report on changes in the environment and support decision-making. The *PAAW* also relates to the natural color of algae in agreement with the earliest classification of phytoplankton by color almost 200 years ago by Harvey (1841) who classified algae in several groups including grass-green, olive-green, yellow, brown, and red. Harvey (1841) also noted the association of color with phytoplankton community structure and affinity to the natural environment. Our index refers only to the color of phytoplankton and does not inform on the bulk optical properties of water as in Vandermeulen et al. (2020) or Gardner et al. (2021), the later focusing on river color using satellite measurements of remote sensing reflectance.

The *PAAW* index could be used for long-term monitoring, as shown by our time series analysis. Decadal and regional analysis of *PAAW* revealed a shift in phytoplankton biomass in spring towards smaller *PAAW* (e.g., blue), suggesting a decrease in the packaging effect and abundance of large phytoplankton such as diatoms. This is consistent with a recent satellite-based study that reveals an overall decrease in large phytoplankton in the biogeochemical provinces of the Northwest Atlantic (Liu et al., 2018). An opposite trend was observed in the autumn on the Scotian Shelf and NAB with a shift of *PAAW* toward the red wavelength, indicating an increase in mean phytoplankton cell size; the shift was particularly important in the NAB. The *PAAW* might be a better indicator than [Chl-a] or a_ϕ(443) to study the impact of climate change on phytoplankton biomass and community structure in agreement with Dutkiewicz et al. (2019) who demonstrated that changes in watercolor, as indicated by remote sensing reflectance, is a better indicator of changes in phytoplankton regimes than biomass as it includes information on changes in community structure. Here, we related *PAAW* to the presence of diatoms and additional studies are required to investigate in detail the relationship between this index and phytoplankton pigment composition in natural samples. However, the *PAAW*, an index that accounts for both phytoplankton biomass and community structure, is easily understandable by a non-expert and provides valuable information on the phytoplankton regime in the marine ecosystem. In fact, no significant trends in a_ϕ (443) were observed in spring in the three regions of the NWA while positives ones were recorded for *PAAW* (Table 2). Our time series analysis showed that the changes in phytoplankton color are not the only bio-optical changes that are occurring in the Northwest Atlantic. At the scale of the NWA, absorption by detritus has increased over the last 20 years by about 1.8 e^{-3} m^{-1} $year^{-1}$, particularly on the Scotian Shelf and NAB in spring. As a result, the contribution of *NAP* to the total particulate absorption has increased.

Our results are consistent with hydrodynamic changes that have been observed over the last two decades in the Northwest Atlantic. The most significant changes occurred on the Scotian Shelf and NAB, which are located at the crossing of subarctic waters from the Labrador Current (i.e., cold, nutrient-rich, and relatively fresh) and deep Atlantic waters (warm, nutrient-depleted, and salty) (Loder et al., 1998; Brickman et al., 2016). These two ecosystems have been subject to a continuous warming over the last decades, particularly in summer and autumn, which has led to an increase in stratification (Hebert et al., 2021). In addition, the warmest water was recorded on the Scotian Shelf and NAB in 2012 (Brickman et al., 2018), indicating a potential shift in the marine ecosystem as supported by our time series analysis. The most significant changes are observed in autumn with a decrease in phytoplankton biomass (Table 2 and Supplementary Figure S5) and phytoplankton becoming greener (Figure 9). This was also associated with an increase in non-algal particle absorption (Supplementary Figure S7) modifying the phytoplankton-*NAP* absorption budget (Supplementary Figure S8). The reasons for such a change are not fully understood and are not within the scope of this study. However, it is noteworthy that changes in *NAP* absorption occurs in both spring and fall while change in the phytoplankton biomass occurs mainly in fall on the Scotian Shelf and NAB, suggesting that different processes are responsible for changes in phytoplankton and *NAP* absorption. Our results are in agreement with Balch et al. (2022) who found a decrease in primary production in the Gulf of Maine also using a 20-year time series. They found that an increase in absorption by dissolved organic matter modified the optical budget of the water column and decreased light availability for phytoplankton photosynthesis associated with an increase in the contribution of nutrient-depleted deep Atlantic water. In the Labrador Sea, we did not find any significant trends in bio-optical properties in spring (Table 2 and Supplementary Figures S5–S8), in agreement with the *PAAW* time series (Figure 9) despite an increase in the nutrient budget that has led to an overall increase of phytoplankton production (Tesdal et al., 2022). The high variability in *PAAW* (and associated bio-optical properties) can be explained by massive phytoplankton blooms that occur at in the Labrador Sea under favorable conditions (e.g., 2015 and 2018 from MODIS-derived spring composite images of [Chl-a]).

Sampling the ocean to study a given phenomenon (e.g., phytoplankton spring bloom) can be challenging given logistic constraints (e.g., ship availability, weather) and the inherent temporal variation of ocean processes. Long-term monitoring programs with dates set in advance mitigate challenges as the repetitive measurements in space and time ensure that most oceanographic conditions will be encountered over years of field measurements. In the case of the spring bloom on the Scotian Shelf, given its variability in time (initiation varies over several weeks) and patchiness, the AZMP spring missions has likely sampled pre- and post-bloom conditions as well as the peak of the bloom, as indicated by the wide range of [Chl-a] (0.1 to 13 mg m^{-3}). The optical relationships found in our study were in agreement with previous models (see Section 3.2) emphasizing the universality of such relationships while also supporting the need to account for regional characteristics for fine-tuning. Our results derived from an extensive dataset explain the good performance of global algorithms such as the Ocean Land Colour Imager (OLCI) Neural Network [Chl-a] algorithm (Hieronymi et al., 2017) or the QAA algorithm (Lee et al., 2002), whose development relied on radiative transfer simulations that included the absorption models of Bricaud et al., 1995; Bricaud et al., 1998; Bricaud et al., 2004). Long-term monitoring program captured the variability in phytoplankton biomass and absorption on the Scotian Shelf in the spring after 5 to 10 years of sampling (Figure 10). Recent trends observed using satellite remote sensing (Liu et al., 2018) might reveal a shift in the timing of phytoplankton growth and assemblage rather than an overall increase of biomass. The most significant changes happen in autumn on the Scotian Shelf and in the NAB with the continuous increase in the standard deviations of the bio-optical properties, which, associated with significant trends over 20 years of observation, indicates that the autumnal ecosystem is still adapting to physical forcing and notably the summer and fall warming up of the water column (Brickman et al., 2018).

5 Conclusion

Our study contributes to the knowledge of bio-optical properties of the Northwest Atlantic and in particular the relationships between phytoplankton biomass and community structure on one side and absorption by phytoplankton and non-algal particles on the other side. The Scotian shelf showed the most seasonal variation in bio-optical properties with the spring and autumn season dominated by large phytoplankton as indicated by low specific absorption and *PAAW*. The NAB showed a similar seasonal cycle to the Scotian Shelf with a lower variability, while the Labrador Sea exhibited a different phenology with a continuous decrease in phytoplankton biomass and an increase in *PAAW* following the spring bloom. Using both traditional phytoplankton-based proxies and the *PAAW* index, results show that the characteristics of the phytoplankton and non-algal absorption in the Northwest Atlantic have undergone significant changes over the past 20 years. The adopted *PAAW* index was found to provide equal or better indications of the phytoplankton community structure compared with metrics that are traditionally measured during oceanographic expeditions. An important aspect in favor of adopting the *PAAW* index is that it is solely based on phytoplankton absorption spectra that are often routinely measured *in situ* by autonomous platforms and profilers. Although additional controlled experiments are needed to evaluate the full potential of *PAAW* to provide insights into phytoplankton biomass and community structure, the results of this study suggest that it could be utilized as an efficient integrative index to obtain information on the health of the marine ecosystem.

Data availability statement

The datasets analyzed in this study are available upon request. It will also be made available on https://www.zenodo.org.

Author contributions

ED designed the study and assembled the dataset. PM computed all the statistics and made all the figures. ED and PM contributed to data analysis and interpretation PM drafted the first version of the manuscript. TP collected the samples and carried out the laboratory analysis. ED and PM iterated the manuscript. TP edited the manuscript. All authors contributed to the article and approved the submitted version.

Funding

This study was supported by the Atlantic Zone Monitoring Program and Atlantic Zone Offshelf Monitoring Program of the Department of Fisheries and Oceans, Canada, particularly the fieldwork and data analysis in the laboratory. This study was made possible thanks to financial support from the Marine Environmental Observation, Prediction and Response Network (MEOPAR). For further information about MEOPAR, visit www.meopar.ca. This research was supported by the Sentinel North program of Universite Laval through salary support for P. Massicotte, made possible, in part, thanks to funding from the Canada First Research Excellence Fund.

Acknowledgments

We are very grateful to the numerous chief scientists, scientists, captains, and crew of the Canadian Coast Guard Ship who have relentlessly relayed over more than 20 years to

build this unique dataset of oceanographic properties. We particularly thank the successive captains and crew of the CCGS Hudson, as this research vessel was used to collect the vast majority of the data presented in the study. The CCGS Hudson was decommissioned in early 2022. We also thank the chairs of the AZMP and AZOMP programs who have supported this research.

Conflict of interest

The authors declare that the research was conducted in the absence of any commercial or financial relationships that could be construed as a potential conflict of interest.

Publisher's note

Supplementary material

The Supplementary Material for this article can be found online at: https://www.frontiersin.org/articles/10.3389/fmars.2022.932184/full#supplementary-material

References

Aiken, J., Hardman-Mountford, N. J., Barlow, R., Fishwick, J. R., Hirata, T., and Smith, T. J. (2007). Functional links between bio-energetics and bio-optical traits of phytoplankton taxonomic groups: an overarching hypothesis with applications for ocean-colour remote sensing. *J. Plankt. Res.* 30, 165–181. doi: 10.1093/plankt/fbm098aiken07

Babin, M., Morel, M., Fournier-Sicre, V., Fell, F., and Stramski, D. (2003). Light scattering properties of marine particles in coastal and open ocean waters as related to the particle mass concentration. *Limnol. Oceanogr.* 48, 843–859. doi: 10.4319/lo.2003.48.2.0843

Balch, W. M., Drapeau, D. T., Bowler, B. C., Record, N. R., Bates, N. R., Pinkham, S., et al. (2022). Changing hydrographic, biogeochemical, and acidification properties in the gulf of maine as measured by the gulf of maine north atlantic time series, gnats, between 1998 and 2018. *J. Geophys. Res.: Biogeosci.* 127, e2022JG006790. doi: 10.1029/2022JG006790

Bidigare, R. R., Morrow, J. H., and Kiefer, D. A. (1989). Derivative analysis of spectral absorption by photosynthetic pigments in the western sargasso sea. *J. Mar. Res.* 47, 323–341. doi: 10.1357/002224089785076325

Brewin, R. J. W., Hardman-Mountford, N. J., Lavender, S. J., Raitsos, D. E., Hirata, T., Uitz, J., et al. (2011). An intercomparison of bio-optical techniques for detecting phytoplankton size class from satellite remote sensing. *Remote Sens. Env.* 115, 325–339. doi: 10.1016/j.rse.2010.09.004

Bricaud, A., Babin, M., Claustre, H., Rase, J., and Tiéche, F. (2010). Light absorption properties and absorption budget of southeast pacific waters. *J. Geophys. Res.: Ocean.* 115, C08009. doi: 10.1029/2009JC005517

Bricaud, A., Babin, M., Morel, A., and Claustre, H. (1995). Variability in the chlorophyll-specific absorption coefficients of natural phtoplankton: Analysis and parameterization. *J. Geophys. Res.* 100, 13321–13332. doi: 10.1029/95JC00463

Bricaud, A., Claustre, H., and Oubelkheir, K. (2004). Natural variability of phytoplankton absorption in oceanic waters: influence of the size structure of algal populations. *J. Geophys. Res. Ocean.* 110, C11010. doi: 10.1029/2004JC002419

Bricaud, A., Mejia, C., Blondeau-Patissier, D., Claustre, H., Thiria, S., and Crepon, M. (2007). Retrieval of pigment concentrations and size structure of algal populations from their absorption spectra using multilayered perceptrons. *Appl. Opt.* 46, 1251–1260. doi: 10.1364/AO.46.001251

Bricaud, A., Morel, A., Babin, M., Allali, K., and Claustre, H. (1998). Variations of light absorption by suspended particles with chlorophyll a concentration in oceanic waters: Analysis and implications for bio-optical models. *J. Geophys. Res.: Ocean.* 103, 31033–31044. doi: 10.1029/98JC02712

Brickman, D., Hebert, D., and Wang, Z. (2018). Mechanism for the recent ocean warming events on the scotian shelf of eastern canada. *Continent. Shelf. Res.* 156, 11–22. doi: 10.1016/j.csr.2018.01.001

Brickman, D., Wang, Z., and DeTracey, B. (2016). Variability of current streams in atlantic canadian waters: A model study. *Atmosphere-Ocean* 54, 218–229. doi: 10.1080/07055900.2015.1094026

Casault, B., Johnson, C., Devred, E., Head, E. J. H., Cogswell, A., and Spry, J. (2020). Optical, chemical, and biological oceanographic conditions on the scotian shelf and in the eastern gulf of maine during 2019. *In. Can. Sci. Advis. Sec. Res. Doc.* 64, 67.

Catlett, D., and Siegel, D. A. (2018). Phytoplankton pigment communities can be modeled using unique relationships with spectral absorption signatures in a dynamic coastal environment. *J. Geophys. Res.: Ocean.* 123, 246–264. doi: 10.1002/2017JC013195

Chase, A., Boss, E., Zaneveld, R., Bricaud, A., Claustre, H., Ras, J., et al. (2013). Decomposition of *in situ* particulate absorption spectra. *Methods Oceanogr.* 7, 110–124. doi: 10.1016/j.mio.2014.02.002

Chazottes, A., Bricaud, A., Crépon, M., and Thiria, S. (2006). Statistical analysis of a database of absorption spectra of phytoplankton and pigment concentrations using self-organizing maps. *Appl. Opt.* 45, 8102–8115. doi: 10.1364/AO.45.008102

Churilova, T., Suslin, V., Krivenko, O., Efimova, T., Moiseeva, N., Mukhanov, V., et al. (2017). Light absorption by phytoplankton in the upper mixed layer of the black sea: Seasonality and parametrization. *Front. Mar. Sci.* 4. doi: 10.3389/fmars.2017.00090

Ciotti, A. M., Cullen, J. J., and Lewis, M. R. (1999). A semi-analytic model of the influence of phytoplankton community structure on the relationship between light attenuation and ocean color. *J. Geophys. Res.* 104, 1559–1578. doi: 10.1029/1998JC900021

Ciotti, A. M., Cullen, J. J., and Lewis, M. R. (2002). Assessment of the relationships between dominant cell size in natural phytoplankton communities and the spectral shape of absorption coefficient. *Limnol. Oceanogr.* 47, 404–417. doi: 10.4319/lo.2002.47.2.0404

Cleveland, J. S. (1995). Regional models for phytoplankton absorption as a function of chlorophyll a concentration. *J. Geophys. Res.* 100, 13333–13344. doi: 10.1029/95JC00532

Collos, Y., Husseini, J. R., Bec, B., Vaquer, A., Lam, H., Rougier, C., et al. (2005). Pheopigment dynamics, zooplankton grazing rates and the autumnal ammonium peak in a mediterranean lagoon. *Hydrobiologia* 550, 83–93. doi: 10.1007/s10750-005-4365-1

Cota, G. F., Harrison, G. W., Platt, T., Sathyendranath, S., and Stuart, V. (2003). Bio-optical properties of the labrador sea. *J. Geophys. Res.: Ocean.* 108 (C7), 3228. doi: 10.1029/2000JC000597

Devred, E., Sathyendranath, S., Stuart, V., Maass, H., Ulloa, O., and Platt, T. (2006). A two-component model of phytoplankton absorption in the open ocean: theory and applications. *J. Geophys. Res.* 111, C03011. doi: 10.1029/2005JC002880

Devred, E., Sathyendranath, S., Stuart, V., and Platt, T. (2011). A three component classification of phytoplankton absorption spectra: Application to ocean-color data. *Remote Sens. Env.* 115, 2255–2266. doi: 10.1016/j.rse.2011.04.025

Dutkiewicz, S., Hickman, A. E., Jahn, O., Henson, S., Beaulieu, C., and Monier, E. (2019). Ocean colour signature of climate change. *Nat. Commun.* 10, 578. doi: 10.1038/s41467-019-08457-x

Duysens, L. M. N. (1956). The flattening of absorption spectrum of suspensions, as compared to that of solutions. *Biochim. Byophys. Acta* 19, 1–12. doi: 10.1016/0006-3002(56)90380-8

Ferreira, A., Ciotti, A. M., Mendes, C. R. B., Uitz, J., and Bricaud, A. (2017). Phytoplankton light absorption and the package effect in relation to photosynthetic and photoprotective pigments in the northern tip of antarctic peninsula. *J. Geophys. Res.: Ocean.* 122, 7344–7363. doi: 10.1002/2017JC012964

Ferreira, A., Stramski, D., Garcia, C. A. E., Garcia, V. M. T., Ciotti, A. M., and Mendes, C. R. B. (2013). Variability in light absorption and scattering of phytoplankton in patagonian waters: Role of community size structure and pigment composition. *J. Geophys. Res.: Ocean.* 118, 698–714. doi: 10.1002/jgrc.20082

Fragoso, G. M., Poulton, A. J., Yashayaev, I., Head, E. J. H., Johnsen, G., and Purdie, D. A. (2018). Diatom biogeography from the labrador sea revealed through a trait-based approach. *Front. Mar. Sci.* 5. doi: 10.3389/fmars.2018.00297

Fragoso, G. M., Poulton, A. J., Yashayaev, I., Head, E. J. H., and Purdie, D. A. (2017). Spring phytoplankton communities of the labrador sea, (2005–2014): pigment signatures, photophysiology and elemental ratios. *Biogeosciences* 14, 1235–1259. doi: 10.5194/bg-14-1235-2017

Fujiki, T., and Tagushi, S. (2002). Variability in chlorophyll a specific absorption coefficient in marine phytoplankton as a function of cell size and irradiance. *J. Plankt. Res.* 24, 859–874. doi: 10.1093/plankt/24.9.859

Gardner, J., Yang, X., Topp, S., Ross, M., Altenau, E., and Pavelsky, T. (2021). The color of rivers. *Geophys. Res. Lett.* 48, e2020GL088946. doi: 10.1029/2020GL088946

Gordon, H. R., and McCluney, W. R. (1975). Estimation of the depth of sunlight penetration in the sea for remote sensing. *Appl. Opt.* 14, 413–416. doi: 10.1364/AO.14.000413

Harvey, W. H. (1841). *A manual of the British algae*. (Paternoster Row, MDCCCXLI, London, England:John Van Voorst)

Head, E. J. H., and Horne, E. P. W. (1993). Pigment transformation and vertical flux in an area of convergence in the north atlantic. *Deep-Sea. Res. II.* 40, 329–346. doi: 10.1016/0967-0645(93)90020-N

Hebert, D., Layton, C., Brickman, D., and Galbraith, P. (2021). Physical oceanographic conditions on the scotian shelf and in the gulf of maine during 2019. *In. Can. Sci. Advis. Sec. Res. Doc.* 2021 (040), 58 p.

Hieronymi, M., Mueller, D., and Doerffer, R. (2017). The olci neural network swarm (onns): A bio-geo-optical algorithm for open ocean and coastal waters. *Front. Mar. Sci.* 4. doi: 10.3389/fmars.2017.00140

Hoepffner, N., and Sathyendranath, S. (1991). Effect of pigment composition on absorption properties of phytoplankton. *Mar. Ecol. Prog. Ser.* 73, 11–23. doi: 10.3354/meps073011

Hoepffner, N., and Sathyendranath, S. (1993). Determination of the major groups of phytoplankton pigments from the absorption spectra of total particulate matter. *J. Geophys. Res.* 98, 22789–22803. doi: 10.1029/93JC01273

IOCCG (2006). *Remote sensing of inherent optical properties: Fundamentals, tests of algorithms, and applications* (Dartmouth, Canada: IOCCG).

Jeffrey, S. W., and Vesk, M. (1997). Introduction to marine phytoplankton and their pigment signatures. In S. W. Jeffrey, R. F.C. Mantoura and S. W. Wright (eds), *Phytoplankton Pigments in Oceanography: A Guide to Advanced Methods*. SCOR-UNESCO, Paris, pp. 37–84

Kirk, J. T. O. (1976). A theoretical analysis of the contribution of algal cells to the atenuation of light within natural waters. *New Phytol.* 77, 341–358. doi: 10.1111/j.1469-8137.1976.tb01524.x

Kratzer, S., and Moore, G. (2018). Inherent optical properties of the baltic sea in comparison to other seas and oceans. *Remote Sens.* 10 (3), 418. doi: 10.3390/rs10030418

Kyewalyanga, M. N., Platt, T., and Sathyendranath, S. (1997). Estimation of the photosynthetic action spectrum: Implication for primary production models. *Mar. Ecol. Prog. Ser.* 146, 207–223. doi: 10.3354/meps146207

Lee, Z. P., Carder, K. L., and Arnone, R. (2002). Deriving inherent optical properties from water color: A multi-band quasi-analytical algorithm for optically deep waters. *Appl. Opt.* 41, 5755–5772. doi: 10.1364/AO.41.005755

Leising, A. W., Pierson, J. J., Halsband-Lenk, C., Horner, R., and Postel, J. (2005). Copepod grazing during spring blooms: Does calanus pacificus avoid harmful diatoms? *Prog. Oceanogr.* 67, 384–405. doi: 10.1016/j.pocean.2005.09.008

Liu, X., Devred, E., and Johnson, C. (2018). Remote sensing of phytoplankton size class in northwest atlantic from 1998 to 2016: Bio-optical algorithms comparison and application. *Remote. Sens.* 10, 1028. doi: 10.3390/rs10071028

Loder, J., Petrie, B., and Gawarkiewicz, G. (1998) vol. 11, 105–133.

Marra, J., Trees, C. C., and O'Reilly, J. E. (2007). Phytoplankton pigment absorption: A strong predictor of primary productivity in the surface ocean. *Deep. Sea. Res. Part I: Oceanogr. Res. Paper.* 54, 155–163. doi: 10.1016/j.dsr.2006.12.001

Mascarenhas, V. J., Voss, D., Wollschlaeger, J., and Zielinski, O. (2017). Fjord light regime: Bio-optical variability, absorption budget, and hyperspectral light availability in sognefjord and trondheimsfjord, norway. *J. Geophys. Res.: Ocean.* 122, 3828–3847. doi: 10.1002/2016JC012610

Matsuoka, A., Babin, M., Doxaran, D., Hooker, S. B., Mitchell, B. G., Bélanger, S., et al. (2014). A synthesis of light absorption properties of the arctic ocean: application to semianalytical estimates of dissolved organic carbon concentrations from space. *Biogeosciences* 11, 3131–3147. doi: 10.5194/bg-11-3131-2014

Mitchell, B. G., and Kiefer, B. A. (1984). "Determination of absorption and fluorescence excitation spectra for phytoplankton," in *Marine phytoplankton and productivity*. Eds. O. Holm-Hansen, L. Bolis and R. Giles (Berlin Heidelberg: Springer-Verlag), 157–169.

Mitchell, B. G., and Kiefer, B. A. (1988). Variability in pigment specific particulate fluorescence and absorption spectra in the northeast pacific ocean. *Deep-Sea. Res.* 28, 1375–1393.

Mobley, C. D. (1994). "Optical properties of water," in *Light and water: Radiative transfer in natural waters*. Eds. O. Holm-Hansen, L. Bolis and R. Giles (London: Academic Press), 61–142.

Morel, A. (1978). Available, usable, and stored radiant energy in relation to marine photosynthesis. *Deep. Sea. Res.* 25, 673–688. doi: 10.1016/0146-6291(78)90623-9

Morel, A., and Bricaud, A. (1981). Theoretical results concerning light absorption in a discrete medium, and application to specific absorption of phytoplankton. *Deep. Sea. Res.* 28, 1375–1393. doi: 10.1016/0198-0149(81)90039-X

Morel, A., and Prieur, L. (1977). Analysis of variation in ocean color. *Limnol. Oceanogr.* 22, 709–722. doi: 10.4319/lo.1977.22.4.0709

Nagasaki, K. (2008). Dinoflagellates, diatoms, and their viruses. *J. Microbiol.* 46, 235–243. doi: 10.1007/s12275-008-0098-y

Nair, A., Sathyendranath, S., Platt, T., Morales, J., Stuart, V., Forget, M. H., et al. (2008). Remote sensing of phytoplankton functional types. *Remote Sens. Env.* 112, 3366–3375. doi: 10.1016/j.rse.2008.01.021

O'Reilly, J. E., Maritorena, S., Mitchell, B. G., Siegel, D. A., Carder, K. L., Garver, S. A., et al. (1998). Ocean color chlorophyll algorithm for SeaWiFS. *J. Geophys. Res.* 103, 24937–24953. doi: 10.1029/98JC02160

Oubelkheir, K., Claustre, H., Bricaud, A., and Babin, M. (2007). Partitioning total spectral absorption in phytoplankton and colored detrital material contributions. *Limnol. Oceanogr.: Methods* 5, 384–395. doi: 10.4319/lom.2007.5.384oubelkheir07

Pepin, P., Petrie, B., Therriault, J.-C., Narayanan, S., Harrisson, W., Frank, K., et al. (2005). The atlantic zone monitoring program (azmp): Review of 1998-2003. *Can. Tech. Rep. Hydrogr. Ocean. Sci.* 242, 57.

Pérez, G. L., Galí, M., Royer, S.-J., Gerea, M., Ortega-Retuerta, E., Gasol, J. M., et al. (2021). Variability of phytoplankton light absorption in stratified waters of the nw mediterranean sea: The interplay between pigment composition and the packaging effect. *Deep. Sea. Res. Part I: Oceanogr. Res. Paper.* 169, 103460. doi: 10.1016/j.dsr.2020.103460

Prieur, L., and Sathyendranath, S. (1981). An optical classification of coastal and oceanic waters based on the specific spectral absorption curves of phytoplankton pigments, dissolved organic matter and other particulate materials. *Limnol. Oceanogr.* 26, 671–689. doi: 10.4319/lo.1981.26.4.0671

Retamal, L., Bonilla, S., and Vincent, W. F. (2008). Optical gradients and phytoplankton production in the mackenzie river and the coastal beaufort sea. *Polar. Biol.* 31, 363–379. doi: 10.1007/s00300-007-0365-0

Sathyendranath, S., Cota, G., Stuart, V., Maass, H., and Platt, T. (2001). Remote sensing of phytoplankton pigments: a comparison of empirical and theoretical approaches. *Int. J. Remote Sens.* 22, 249–273. doi: 10.1080/014311601449925

Sathyendranath, S., Watts, L., Devred, E., Platt, T., Caverhill, C., and Maass, H. (2004). Discrimination of diatoms from other phytoplankton using ocean-color data. *Mar. Ecol. Prog. Ser.* 272, 59–68. doi: 10.3354/meps272059

Shuman, F. R., and Lorenzen, C. J. (1975). Quantitative degradation of chlorophyll by a marine herbivore. *Limnol. Oceanogr.* 20, 580–586. doi: 10.4319/lo.1975.20.4.0580

Sosik, H. M., and Mitchell, B. G. (1992). A comparison of particulate absorption properties between high- and mid-latitude surface waters. *Antarctic. J. Unit. States* 27, 162–164.

Staehr, A., Markager, S., and Sand-Jensen, K. (2004). Pigment specific *in vivo* light absorption of phytoplankton from estuarine, coastal and oceanic waters. *Mar. Ecol. Prog. Ser.* 275, 115–128. doi: 10.3354/meps275115

Stramski, D., Reynolds, R. A., Kaczmarek, S., Uitz, J., and Zheng, G. (2015). Correction of pathlength amplification in the filter-pad technique for measurements of particulate absorption coefficient in the visible spectral region. *Appl. Opt.* 54, 6763–6782. doi: 10.1364/AO.54.006763

Stuart, V., and Head, E. J. H. (2005). "The BIO method," in *The second SeaWiFS HPLC analysis round-robin experiment (SeaHARRE-2)*, vol. 112 . Ed. S. B. Hooker (Greenbelt, Maryland: NASA/TM 2005-212785).

Stuart, V., Sathyendranath, S., Head, E. J. H., Platt, T., Irwin, B. D., and Maas, H. (2000). Bio-optical characteristics of diatom and prymnesiophyte populations in the Labrador Sea. *Mar. Ecol. Prog. Ser.* 201, 91–106. doi: 10.3354/meps201091

Stuart, V., Sathyendranath, S., Platt, T., Maass, H., and Irwin, B. D. (1998). Pigments and species compositon of natural phytoplankton populations: effect on the absorption spectra. *J. Plankt. Res.* 20, 187–217. doi: 10.1093/plankt/20.2.187

Teegarden, G. J., Campbell, R. G., and Durbin, E. G. (2001). Zooplankton feeding behavior and particle selection in natural plankton assemblages containing toxic alexandrium spp. *Mar. Ecol. Prog. Ser.* 218, 213–226. doi: 10.3354/meps218213

Tesdal, J.-E., Ducklow, H. W., Goes, J. I., and Yashayaev, I. (2022). Recent nutrient enrichment and high biological productivity in the labrador sea is tied to enhanced winter convection. *Prog. Oceanogr.* 206, 102848. doi: 10.1016/j.pocean.2022.102848

Therriault, J.-C., Petrie, B., P. Pépin, J. G., Gregory, D., Helbig, J., Herman, A., et al. (1998). Proposal for a northwest atlantic zonal monitoring program. *Can. Tech. Rep. Hydrogr. Ocean. Sci.* 194, 57.

Trees, C. C., Clark, D. K., Bidigare, R. R., Ondrusek, M. E., and Mueller, J. L. (2000). Accessory pigments versus chlorophyll a concentrations within the euphotic zone: An ubiquitous relationship. *Limnol. Oceanogr.* 45, 1130–1143. doi: 10.4319/lo.2000.45.5.1130

Trzcinski, M. K., Devred, E., Platt, T., and Sathyendranath, S. (2013). Variation in ocean colour may help predict cod and haddock recruitment. *Mar. Ecol. Prog. Ser.* 491, 187–197. doi: 10.3354/meps10451

Vandermeulen, R. A., Mannino, A., Craig, S. E., and Werdell, P. J. (2020). 150 shades of green: Using the full spectrum of remote sensing reflectance to elucidate color shifts in the ocean. *Remote Sens. Environ.* 247, 111900. doi: 10.1016/j.rse.2020.111900

Vishnu, P., Shaju, S., Tiwari, S., Menon, N., Nashad, M., Joseph, C. A., et al. (2018). Seasonal variability in bio-optical properties along the coastal waters off cochin. *Int. J. Appl. Earth Observat. Geoinform.* 66, 184–195. doi: 10.1016/j.jag.2017.12.002

Williams, G. N., Larouche, P., Dogliotti, A. I., and Latorre, M. P. (2018). Light absorption by phytoplankton, non-algal particles, and dissolved organic matter in san jorge gulf in summer. *Oceanography* 31, 40–49. doi: 10.5670/oceanog.2018.409

Wu, Y., Platt, T., Tang, C., Sathyendranath, S., Devred, E., and Gu, S. (2008). A summer phytoplankton bloom triggered by high wind events in the Labrador Sea, july 2006. *Geophys. Res. Lett.* 35. doi: 10.1029/2008GL033561

Zang, Z., Ji, R., Liu, Y., Chen, C., Li, Y., Li, S., et al. (2022). Remote silicate supply regulates spring phytoplankton bloom magnitude in the gulf of maine. *Limnol. Oceanogr. Lett.* 7, 277–285. doi: 10.1002/lol2.10245

Zhang, Y., Wang, G., Sathyendranath, S., Xu, W., Xiao, Y., and Jiang, L. (2021). Retrieval of phytoplankton pigment composition from their *in vivo* absorption spectra. *Remote Sens.* 13 (24), 5112. doi: 10.3390/rs13245112